SpaceSkin: development of aerospace-grade electronic textile for simultaneous protection and high velocity impact characterization

Cherston, Juliana, Paradiso, Joseph

Juliana Cherston, Joseph A. Paradiso, "SpaceSkin: development of aerospace-grade electronic textile for simultaneous protection and high velocity impact characterization," Proc. SPIE 10970, Sensors and Smart Structures Technologies for Civil, Mechanical, and Aerospace Systems 2019, 109700J (27 March 2019); doi: 10.1117/12.2513962

SPIE.

Event: SPIE Smart Structures + Nondestructive Evaluation, 2019, Denver, Colorado, United States

SpaceSkin - development of aerospace-grade electronic textile for simultaneous protection and high velocity impact characterization

Juliana Cherston[a] and Joseph A. Paradiso[a]

[a]MIT Media Lab Responsive Environments Group, 75 Amherst Street, Cambridge MA, USA

ABSTRACT

This paper introduces the concept of an aerospace-grade electronic textile and summarizes design studies and early prototype development for on-fabric hypervelocity impact characterization. Whereas most damage detection technologies for aerospace systems rely on enhancements to the structure's inner shell, the outermost protective skin of a space habitat or a spacesuit - traditionally a woven fabric - is directly exposed to the relevant environment. Therefore, we propose weaving sensory fibers into traditional fibrous aerospace skins for direct measurement of local conditions, yielding a material that can simultaneously sense and protect. Specifically, this paper documents design considerations for multifunctional Beta cloth, in which piezoelectric yarn is directly woven into Teflon-coated fiberglass, the material used as the outermost skin of the International Space Station. A review of hypervelocity plasma generation then motivates a strawman design for on-textile plasma charge and RF emission sensing, which may be useful for further characterization of hypervelocity impactors. An aerospace-grade electronic textile is distinct from a traditional e-textile in that it must be validated not only for its sensing capabilities but also for its robustness to hazards presented in a space environment.

Keywords: electronic textiles,aerospace skin,damage detection,smart fabrics, smart fibers,multifunctional systems,aerospace materials,space structures

1. INTRODUCTION

It is well known that the space environment is hazardous to man-made assets ranging from habitats to spacesuits. Threats include ionizing radiation, UV radiation, thermal cycling, atomic oxygen erosion, and high velocity impact. As such, the outermost protective skin of a persistent resource - often a tightly woven textile material - is designed with consideration for its longevity. For example, the exterior of the International Space Station is composed of Teflon-coated fiberglass ('Beta cloth') which is resilient to atomic oxygen erosion and designed for combined strength, durability, and flame resistance. Similarly, the outermost skin of a spacesuit is frequently composed of a Nomex, Gore-Tex, and Kevlar blend ('Ortho-fabric'), which balances flexibility with resilience (see Figure 1).*

Though these two representative protective materials benefit from decades of flight heritage, they remain notably passive, despite offering key real-estate on the spacecraft for active sensing and actuation during long duration missions. Inspired by advances in electronic textiles, we propose modifying the outermost skin of a persistent space structure to simultaneously sense and protect, emulating the dual protective and sensory capabilities of biological skin. As a first application area, we focus on developing a modified Beta cloth fabric that can localize and characterize high velocity impact while preserving protective material properties critical to the mission's long term success.

This proposal follows the principle of multifunctional (or 'integrated') design, an emerging paradigm in aerospace engineering which optimizes for savings in mass, volume and touch labor by embedding disparate functionalities into single subsystems.[1,2]

Further author information: (Send correspondence to)
Juliana Cherston: E-mail: cherston@mit.edu

*Assets with shorter total deployment time will often use thin film skins made of e.g. Teflon or coated Kapton

Sensors and Smart Structures Technologies for Civil, Mechanical, and Aerospace Systems 2019, edited by Jerome P. Lynch, Haiying Huang, Hoon Sohn, Kon-Well Wang, Proc. of SPIE Vol. 10970, 109700J
 · doi: 10.1117/12.2513962

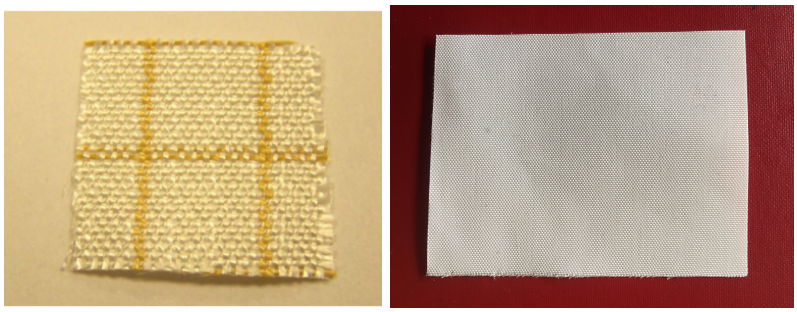

Figure 1. Heritage aerospace-grade textile skins - Ortho-fabric: outermost protective layer of spacesuit (left) Beta cloth, outermost protective layer of space station (right)

There are two key aspirations for on-skin detection of hypervelocity impact:

(1) **Damage Detection** Damage induced by impactors can be substantial, even for micron-scale impactors. For instance, an 100 micron diameter micrometeoroid with density $0.5 g/cm^3$ traveling at 20 km/s will impart 20 μJ of energy in a very concentrated region (see [3] for impact effect by size and subsystem). Knowledge of the location and severity of hypervelocity impact can aid in swifter diagnosis and repair of space-based assets. As the skin covers a large swath of the satellite's exterior, it is a suitable candidate for large area sensing.

(2) **Scientific Contribution** If a standardized, active skin is widely adopted as an alternative to today's passive material, there may be an opportunity to collect sizeable dataset of impactor distribution across the solar system with spatial and temporal resolution. Further, characterization of the composition of natural impactors would allow for a more expansive search for space dust containing either organic compounds or amino acids, of interest for theories on interplanetary transfer of the seeds of life. A skin may also prove more sensitive to non-penetrating impact events in comparison to composite sensors embedded in the spacecraft's walls.

This work is complementary to the JAXA/ISAS CLOTH project in which dust detectors are embedded in one of the inner layers of MLI, sharing a similar goal of turning the thermal blanket of a spacecraft into a large area dust detector.[4]

2. AEROSPACE GRADE ELECTRONIC TEXTILE DESIGN CONSIDERATIONS

2.1 Typical Multilayer Insulation (MLI) Design Considerations

In order to reduce heat loss, spacecraft are very often wrapped in multilayer insulation (MLI) consisting of layers of metalized film with thermally insulating mesh spacers. The design of MLI is largely dictated by the environmental conditions to which the spacecraft will be exposed.[5] In general, it is well known that the outermost layer of MLI must be specified with care. This lesson was learned the hard way - the Teflon sun shield of the NATO II satellite and the Teflon MLI blankets of the Hubble Space telescope each experienced tears due to thermal cycling and bombardment by charged particles and - critically - by atomic oxygen (AO). AO erosion yield is calculated as:[6]

$$E_y = \frac{t_i - t_f \rho_f / \rho_i}{F} \tag{1}$$

Where t_f and t_i correspond to initial and final thickness, ρ_f and ρ_i correspond to initial and final density, and F corresponds to atomic oxygen fluence. It poses one of the most severe and consistent threats to persistent space structures deployed in Low Earth Orbit. A densely woven fiber minimizes AO penetration risk and preserves some robustness to impact. Teflon coated fiberglass is often selected for its chemical inertness, and its white color is beneficial for thermal regulation.

Once an outer material's robustness to AO erosion is proven, it must also be shown to generate a minimum amount of particulate contaminants and tolerate thermal cycling anticipated for the deployment scenario. In cases where electrostatic charging is critical, the outer layer will also be coated in indium tin oxide, a conductive

coating which, when grounded, offers a discharge path from the surface. Finally, the overall blanket's performance will be evaluated by its absorption to emittance (α/ϵ) ratio, which is used to determine the thermal response of the system to sunlight. The outermost layer will strongly influence this parameter. For detailed discussion on further MLI design considerations, consult e.g. 5.

2.2 Aerospace-Grade Electronic Textile Design Considerations

Electronic textiles are in active development for applications in on-body sensing[7] and responsive fashion,[8] but their benefits have yet to be exploited in an aerospace context. An aerospace-grade textile may draw heavily from existing fiber technologies. For example, by eventually integrating textile solar cells and textile antennas into the fabric, the skin may operate as an autonomous system in relation to the host craft, and thus be readily integrated into diverse space assets and widely deployed. However, an additional design constraint must be met: the material's robustness to spaceborne threats and maintenance of MLI performance must be demonstrated in addition to its sensing capabilities. Therefore, example design considerations for space-exposed electronic textiles are listed below:

- Higher density fabrics show improved erosion resistance and marginal improvements to impact resistance. Therefore, woven fabrics are often preferred to knitted fabrics
- the electronic textile must not store charge or voltage on its surface, as spacecraft charging poses substantial risk for ESD events that are harmful to spacecraft electronics
- Sensor performance must either tolerate or compensate for substantial thermal cycling, shielding any secondary components as needed
- Radiative heat transfer should be minimized by preserving low absorption-emittance properties of the outer layer (often a white fabric is preferred, seams are minimized to prevent heat loss, and the blanket is kept loose to minimize thermal contact between layers)
- Cutouts in MLI are usually required for protruding spacecraft parts, and persistent space habitats and spacesuits have unique geometries. Electronic textiles must be able to tolerate variable geometries and potentially also cutting
- Abrasion resistance is important for fabrics coming into contact with rough surfaces and must be preserved (e.g. Chromel-R, a woven stainless steel, is used on Lunar EVA gloves)

2.3 Candidate Hypervelocity Sensing Approaches and Design Considerations

Returning to applications specifically in impact characterization, we note that a hypervelocity impact is characterized by the following measurable effects:

- Electromagnetic emissions (e.g. visible light flash, infrared radiation, microwave radiation)
- Shock induced acceleration
- Acoustic vibration within the impacted structure
- Secondary debris clouds
- Plasma clouds and ejecta
- Crater or hole with associated size, shape, and location
- Chemical / crater material residue

As a primary goal, we are developing piezoelectric fiber that can be woven directly into Beta cloth at intervals narrow enough to ensure acoustic transmission through the material and sparse enough to sufficiently preserve the well-known tolerance of Beta Cloth to space conditions.[9,10] The sensor response will be characterized in high velocity impact testing facilities, and the material will be evaluated for its robustness to thermal cycling, ultraviolet radiation, and atomic oxygen exposure. The modified material will be compared to two benchmarks: traditional Beta cloth and a simple Beta cloth piezo-film laminate. We are also developing supporting low power electronics for amplification, filtering, and data capture.

As a secondary goal, we are reviewing candidate textile sensing methods for characterizing the composition of impactors. Most simply, the system will discriminate between impactors of natural and manmade origin using measurements of velocity inferred from piezoelectric measurements. A step further would be to approximate dominant constituent elements: according to LDEF and Hubble post flight analysis, micrometeoroids are dominated by silicate minerals, calcite, metal sulfides, and various iron containing compounds often dating back to the birth of the solar system. Conversely, debris of man-made origin is dominated by aluminum, aluminum oxide, specialized steels, and paint fragments.[11] In Section 5 we explore performing coarse characterization of impactor composition by measuring charge deposition and RF emission from the plasma formed during impact. Note that there may also be approaches for measuring trace presence of organic chemicals using techniques in chemical sensing including conducting polymer sensors and chemiresistors, though sensor response times - on the scale of minutes - are likely too slow for the given application, so this approach is only briefly mentioned.

3. PRIOR ART

3.1 MLI Passive Functionality

Prior work incorporating passive functionality into a spacecraft's MLI include the Toughened Thermal Blanket, which introduces a layer of Nextel ceramic cloth just behind the top of the thermal blanked cover for added robustness,[12] and the Stuffed Whipple Shield, which offers additional radiation protection to an impact shield.[13]

3.2 MLI Active Functionality

The I-Suit from ILC Dover back in 2003 integrated pressure sensitive textile switches into the glove of a spacesuit for rover control, and in the shoulder for helmet lighting control.[14] It is the only known exploration of the integration of active sensors into the outermost aerospace-grade textile material. Otherwise, two projects are known that propose to embed thin film sensors *inside* MLI: the SanSEc project proposed substituting an open circuit thin film resonant sensor as an MLI inner layer for damage detection,[15] and the CLOTH project from JAXA embeds thin film PVDF for impact detection.[16] In these cases, the sensor is shielded from the space environment and only effects on MLI performance need to be considered.

3.3 Hypervelocity Impact Detection

In-situ impact detection using dedicated detectors is commonplace.[17] A variety of sensing techniques are used. See for example the DRAGONS Acoustic/Resistive Impact Detector,[18] ALADDIN Acoustic Detector,[19] Hyperdust Chemical Sensor,[20] and HELIOS Mass Spectrometer,[21] among others). However, these detectors require that the micrometeoroid strikes within the sensor's aperture. Some strikes have also been inferred by interpreting noise in subsystems (e.g. see SOLID Solar Panel Detector[22]).

3.4 Piezoelectric Fibers

Piezoelectric fibers have yet to be studied or tested in an aerospace context. More broadly, while rigid piezoelectric composites have been substantially explored, textile piezoelectrics have only been studied over the last few years for applications in wearable technology, and there are substantial engineering challenges involved in manufacturing precision multimaterial fibers as well as activating their sensory capabilities, as will be shown experimentally in the next section.[23–26]

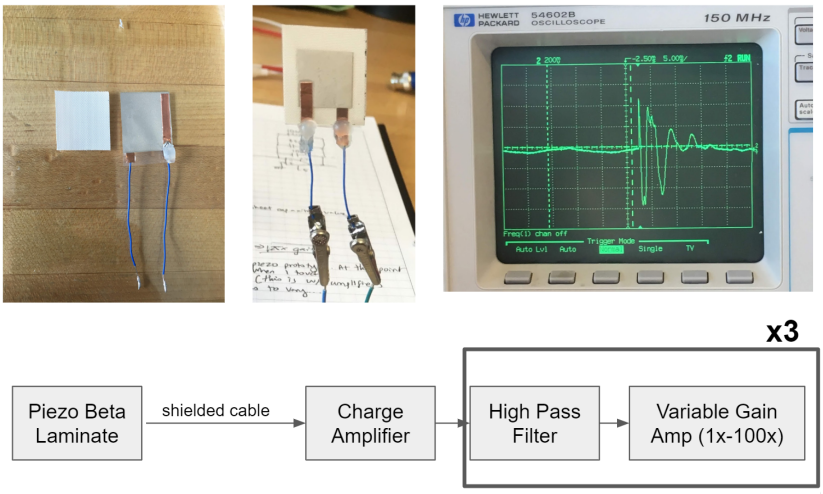

Figure 2. (Left) Piezofilm and beta cloth (middle) Beta cloth piezo film laminate (right) film sensor response to mechanical stimulation (bottom) amplification/filtering electronics

4. PIEZOELECTRIC FIBER DEVELOPMENT PROCESS

4.1 Beta Cloth + PVDF Laminate For Benchmarking

Piezoelectric Beta Cloth sensor performance will ultimately be benchmarked against the more standard manufacturing approach of laminating piezoelectric thin film onto the desired substrate. A laminate control sample was our first prototype - consisting of piezoelectric film laminated with polypropyline onto Beta Cloth. The laminate was paired with basic filtering and amplification circuitry (see block diagram in Figure 4.1) and shown to produce a measurable signal when subject to impact from a 1 km/s, 20 micron steel particle. A detailed characterization of fiber sensors and control laminates subject to high velocity impact will be treated in a separate paper.

4.2 Study on use of commercial monocomponent PVDF yarn

While piezoelectric coaxial cable has a long history, there are no commercial piezoelectric yarns available. A small number of manufacturers have recently commercialized Kynar PVDF yarn optimized for physical and chemical characteristics rather than piezoelectric response. We evaluated whether a multifilament yarn sample donated by MiniFibers Inc was suitable for use as a sensor component. Firstly, the yarn must be shown to contain sufficiently high crystalline beta phase concentration. This might generally be anticipated for PVDF in yarn form, as linear stress tends to yield preferential beta alignment.[26] Secondly, it must be possible to weave the fiber into a fabric and apply conductive charge collection layers to the surfaces of the material using e.g. stretchable conductive ink as an interface. Thirdly, a poling voltage greater than the coercive field strength of PVDF must be achieved and sustained in order to permanently align dipoles across a two dimensional array of fibers. Poling above the material's coercive field strength also has potential to further increase beta alignment.

4.2.1 Phase Alignment Measurements

Figure 3 shows X-ray diffraction images of the yarn, which allows for qualitative evaluation of phase distrbutions. The peak at $2\theta = 20.26°$is related to the diffraction of β phase at (110) and (200) crystal planes. Meanwhile, the peaks at 18.3°and 26.5°are indicative of alpha phase at (020) and (021) crystal plane, respectively. No indication of gamma phase alignment ($2\theta = 18.5, 19.2, 20.0$) are present in the data.

Fourier Transform Infrared Spectroscopy (FTIR) is used to quantify the distribution of phases in the material. Results are shown in Figure 4. Assuming that absorption follows the Lambert-Beer Law,[27] the following derived relation is commonly used to calculate the relative fraction of beta phase in PVDF:

$$F(\beta) = \frac{A_\beta}{(K_\beta/K_\alpha)A_\alpha + A_\beta} \tag{2}$$

Where A_β is the absorption at 840nm, A_α is the absorption at 766nm, and K is the absorptivity at the respective wave number. Averaging across five FTIR images for unpoled PVDF samples, we calculate a beta phase concentration of approximately 78.5%. For comparison, PVDF thin films generally do not exceed 80% relative beta fraction.[28] See also [29] for a useful flowchart for deriving relative phase concentrations from FTIR data. Based on XRD and FTIR analysis, we conclude that this yarn has sufficient beta alignment for use as a sensor.

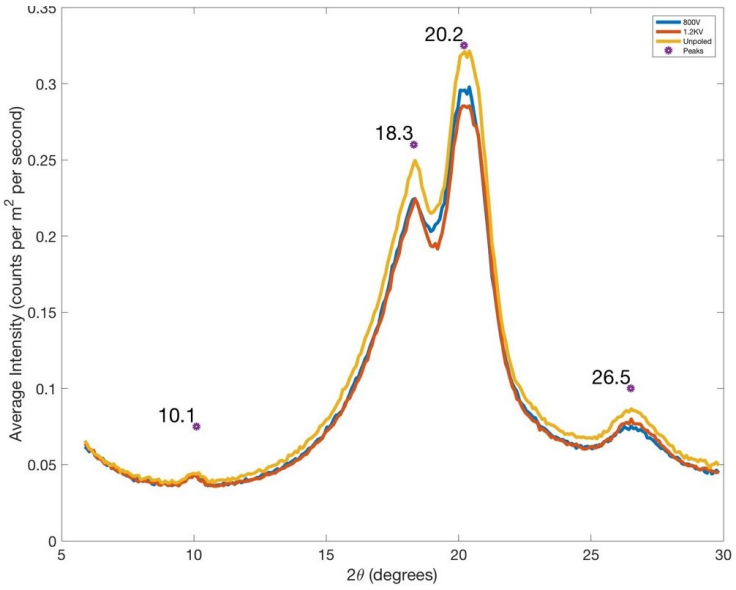

Figure 3. X-ray diffraction image of unpoled commercial PVDF fiber. The peak at $2\theta = 20.26°$is related to the diffraction of β phase at (110) and (200) crystal planes. The peaks at 18.3°and 26.5°are indicative of alpha phase at (020) and (021) crystal plane, respectively.

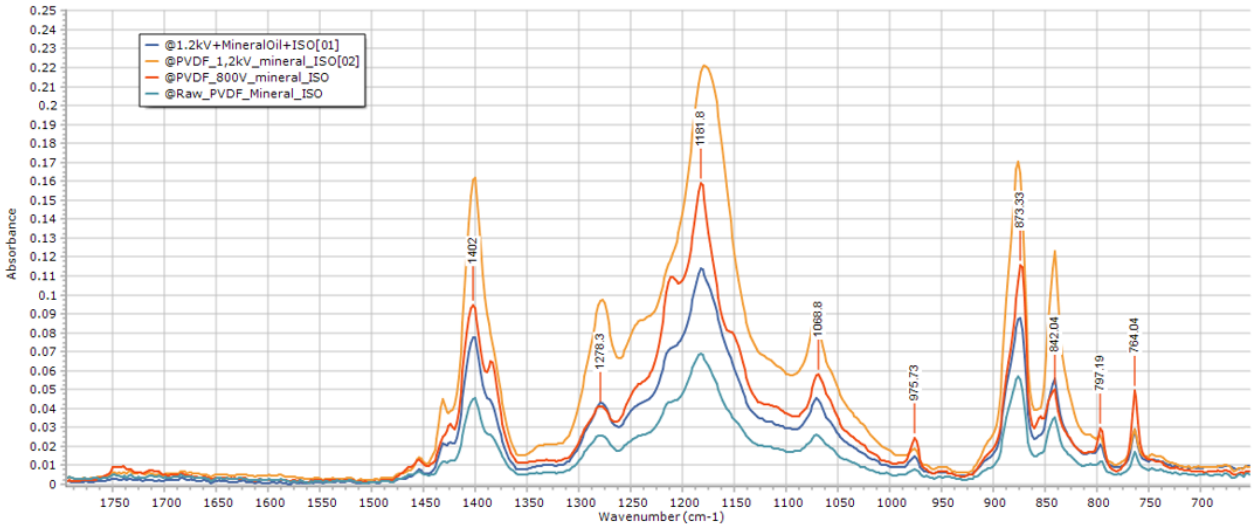

Figure 4. Fourier transform infrared spectroscopy for PVDF yarn samples. Beta phase concentration calculated to 78.5%. Little change in spectral signatures when subject to a range of electric field strengths, suggesting that no additional beta alignment is induced from poling.

4.2.2 Conductive Ink/Stenciling Process Evaluation

Secondly, we hand wove the yarn into a fabric and tested the fabric's ability to support a strechable conductive ink coating. We found strong adhesion and measured resistivity to be 0.1 $\Omega \cdot m$ across centimeter-scale distances using EMS CI-1036 silver conductive ink stenciled onto a fabric containing PVDF yarn interlaced with Teflon coated fiberglass. Process photos are shown in Figure 5.

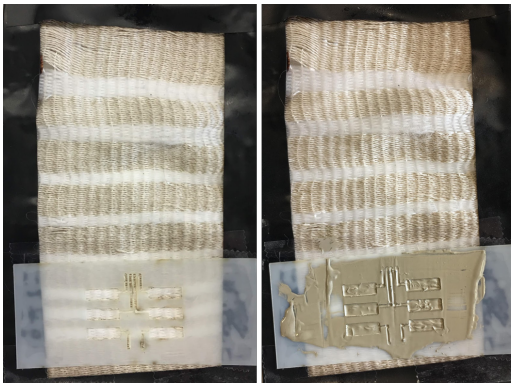

Figure 5. Process photo showing stenciling of conductive ink onto PVDF substrate for evaluation of adhesion and resistivity

4.2.3 Poling For Dipole Alignment

Although sufficient beta alignment is present along the yarn, inter-yarn dipole alignment within the fabric is critical as well for constructive interference of fiber sensor response. Therefore, a poling process must be carried out to permanently align dipoles across a two dimensional fabric. PVDF behaves as a ferroelectric below the Curie temperature of 195°C. The hysteresis curve that defines phase changes for PVDF is well characterized and defined by Equation 3.[30,31]

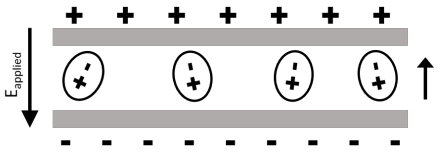

Figure 6. Electric field applied to align dipoles

$$\frac{dF_p}{dt} = \alpha(T - T_c)P + bP^3 + cP^5 = E. \tag{3}$$

This expression is derived by Taylor expanding the Gibbs free energy expression with polarization as an order parameter, minimizing free energy at thermal equilibrium, and applying work term **EP** - derived from Maxwell's equations - for the external electric field. To induce permanent alignment of dipoles, a voltage above the coercive field strength, as approximated using Equation 3, must be applied at elevated temperature. The coercive field strength of PVDF ranges from 50 MV/m to 90 MV/m in the literature. However, the application of this field to an inherently porous fabric or fiber array is limited by the dielectric breakdown strength of the medium. (Conversely, the breakdown strength of PVDF is approximately 770 MV/m - thus the poling of nonporous thin films is readily achieved).

An experimental compaign was conducted to see whether coercive field strengths could be achieved using porous fabric and yarn. Samples of PVDF yarn were laid flat in between two conductive plates. Both rigid copper plates and copper tape were tested. Experimental setup is shown in Figure 4.2.3. PVDF yarn thickness

Dielectric	Quoted Breakdown Strength (MV/m)	Observed Breakdown Strength (MV/m)
Air	3	3±1
Mineral Oil[32]	12	10±3
Dielectric Grease[33]	43	8±5
Castor Oil[32]	65	15±4

Table 1. Summary of dielectrics tested with comparison of breakdown strength quoted in the literature and experimentally measured breakdown strength

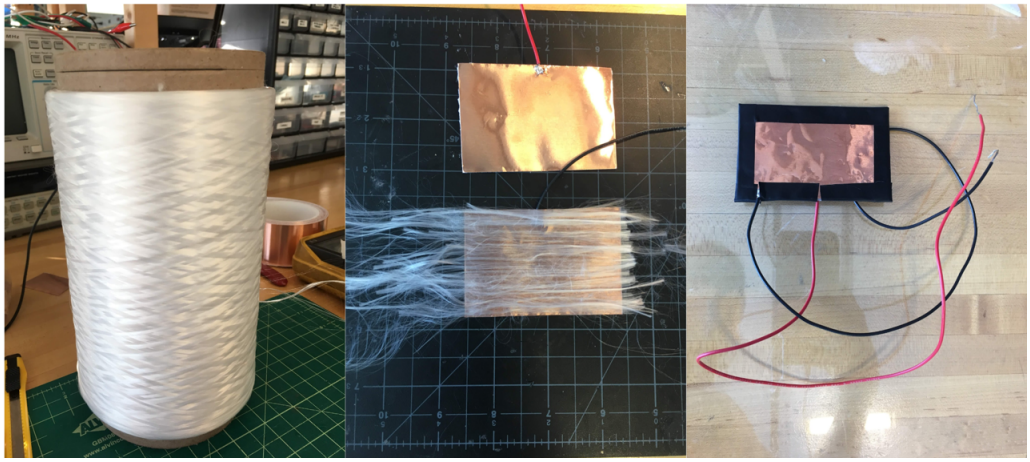

Figure 7. Left: PVDF yarn. Middle: Yarn laid in an array on conductive plate. Right: Assembled PVDF specimen ready for poling

varied from 100 microns to 300 microns and a constant elevated temperature was applied ranging from 60 degrees to 100 degrees in different trials. The samples were placed in baths using the dielectrics listed in table 4.2.3 in order to increase poling voltage, and were subsequently cleaned using IPA. A DC voltage was applied to the copper plates using a Hipotronics HD100 Hipot tester in order to produce a constant electric field.

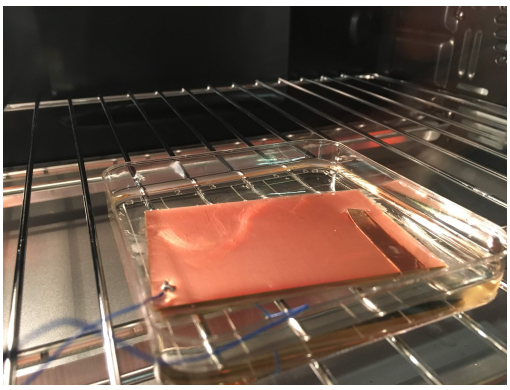

Figure 8. example configuration of sample in heated dielectric bath

However, in all experiments using liquid dielectrics, field strengths ranging only up to 15 MV/m were achieved before arcing, still significantly below the coercive field strength of PVDF and also below the rated dielectric breakdown strength for dielectric grease and castor oil. Nonuniformities in thickness of the yarn arrays and fabrics may also have substantial impact on achievable field strengths. Arcing across fringe fields may also be partially responsible for explaining this discrepancy.

Despite E-field strengths below the coercive field requirement, samples were manually tested for any piezoelectric response. As anticipated, in all cases, a response was either not seen or only temporarily seen over

a 30 minute period following poling, which may either be due to charge temporarily accumulated during the application of an electric field or due to a temporary dipole alignment followed by gradual relaxation that is typical of a material poled below its coercive field strength. If subtle piezoelectric responses did remain, they were dominated by capacitive effects that were equally present in unpoled control samples.

Other geometries tested included a corespun fiber (in which PVDF yarn is wrapped around a central conductive filament), knitted yarn, and stacked dielectrics. For instance, when layering 50 micron thickness kapton film on top of the yarn in a castor oil bath, field strengths of 55 MV/m are achieved, but in this stacked configuration the field strength across the yarn layer is only expected to be at most 36 MV/m, still well below coercive field strengths required.

We conclude that it is sub-optimal, and possibly infeasible, to use commercial single material PVDF yarn for piezoelectric fabric design due principally to the material's porosity and nonuniformity. There is a possibility that PVDF fabric with very fine yarn and very uniform thickness might better tolerate elevated electric field.

4.3 Piezoelectric Fiber Device Development

Given that no piezoelectric yarn is commercially available, we turn instead to manufacturing of custom piezoelectric yarn with conductive cores and conductive ink coating. This modification, which is in progress, will ease the poling process by applying voltage across a continuous layer of piezoelectric material, rather than across a sparse fabric layer.

5. EMP AND RF EMISSION FROM PLASMA: REVIEW AND DESIGN STUDY

In this section, we present a review of EMP and RF emission due to impact plasma followed by a strawman design for an on-textile plasma sensor.

5.1 Overview of Plasma generation during hypervelocity impact

When subject to impact speeds exceeding approximately 8 km/s, impactors will ionize and generate a highly localized plasma. The plasma rapidly expands into the vacuum with expansion velocity V_e between 10km/s to 30km/s, expending thermal energy to gain kinetic energy.[34]

Following ionization, electrons expand faster than ions, creating an ambipolar electric field which draws electrons back towards the ions. Electrons will thus oscillate about the ion front at the plasma frequency, which is density dependent and will decrease over time. This effect can be described by a chirp function with initial frequency dependent on initial ion density and the rate dependent on plasma density fall off.[35] Further, an impact tends to generate melt and fragmental debris. According to [36], if this debris comes into contact with the plasma, it will tend to pick up electrons and acquire a negative charge, resulting in macroscale charge separation. However, according to [37], attachment of charge to particulates may be unlikely due to plasma temperatures exceeding 10 eV.

For a 100 micron particle, the average plasma timescale is on the order of microseconds, and the average size is on the scale of millimeters, though time and length scales are heavily velocity dependent. See Figure 3 in [38] for additional detail.

Plasmas will frequently be modeled using simplifying approximations that eliminate interplay between internal and external electromagnetic fields. It can be shown that the ratio between the plasma frequency and ion collision frequency yields the relation:

$$\frac{\omega_p}{\nu} \propto \sqrt{\frac{T^3}{n}} \tag{4}$$

where n is the plasma density and T is the plasma temperature. Based on Equation 4, a low density, high temperature plasma can be treated as a single conducting fluid subject only to external electric and magnetic fields ('collisionless, ideal plasma'). Conversely, inter-particle effects will often dominate for high density, low temperature plasmas ('collisional plasma'). The plasma generated during a hypervelocity impact has high density and low temperature, and is thus strongly non-ideal - field/particle coupling understood using Maxwell's Equations

imply that charged particles in the plasma both create an electromagnetic field and are strongly influenced by it. However, once the plasma has expanded to a collisionless state, it takes on ideal properties.[39] Finally, the total amount of charge (q) deposited from a hypervelocity impact has been empirically shown to follow the power law:[37]

$$q \propto mv^{3.8} \tag{5}$$

5.1.1 Plasma RF Emission

At speeds above 18 km/s, the plasma substantially ionizes and will have a tendency to expand until collisionless (at lower velocities, recombination will be favored). In this >18 km/s velocity domain, radio frequency emissions have also been detected, with detection rates approaching 75% as impact speed approaches 72 km/s. However, at speeds below 18 km/s, recombination dominates and RF emission is rarely detected. These velocity regimes are summarized graphically in Figure 5.1.1.

This RF emission phenomenon was first observed by Bianchi et al,[40] and the pulses generated by dust impacts were first discovered using electric field measurements in the vicinity of Saturn's ring plane by the Voyager spacecraft. There is no firm consensus on the physical mechanism for this RF emission, and some discrepancy in the literature regarding conditions required to produce it, though it appears to require substantial ionization of the plasma and may require a electrically biased target object. The emission is presumably related to charge motion in the plasma, and some type of instability only present under certain conditions. According to Close et al., the RF emission is thought to present once the collision frequency and plasma frequency are equal, at which point surface electrons are able to separate from the plasma and oscillate significantly in-phase.[37] Microcracking of the target material in ground experiments will also generate plasma in high mass, low velocity regimes.

Because space debris travels at 7 to 12 km/s and micrometeoroids travel at 11 to 72 km/s, the presence of a plasma suggests an impactor of natural origin.

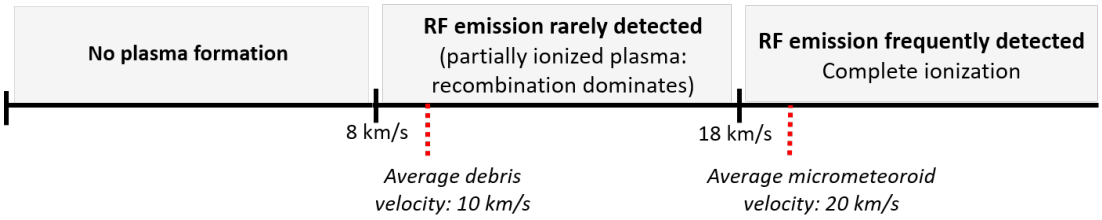

Figure 9. Simplified schematic showing velocity regimes in which RF emission has been detected, with average debris and micrometeoroid impact velocity labeled for reference

5.1.2 Plasma Sensing

In prior ground experiments, plasma is often measured using a retarding potential analyzer (RPA), which is a planar ion trap that captures selectively filtered ions via a varying grid potential. Only ions with energy-to-charge ratios $\frac{E}{q}$ greater than the grid voltage can pass through the grid apertures to reach the collector. The magnitude of the derivative of the resulting I-V curve is proportional to the ion energy distribution. Multiple distinct peaks can sometimes be attributed to separated ion species, which have differing time of flight to the RPA.[35] Additionally, photomultiplier tubes can be used to detect the optical flash that occurs on impact, and conducting plate arrays can be used to measure degree of charge separation as well as the spatial extent and velocity distribution of the charged debris based on ion species mobility. Further, low frequency planar antennas can be used to pick up RF emission. For example, Close et al used quarter wave chip planar antennas tuned to hundreds of MHz and positioned tens of centimeters away from the target. A field strength of 1.9 V/m was measured by the antennas at 30cm from the point of impact, with generally stronger returns at 315 MHz than at 916MHz. In this experiment, RF emission was rarely detected for grounded targets, but routinely detected from high speed particles impacting highly biased targets ($\pm 1kV$).[41]

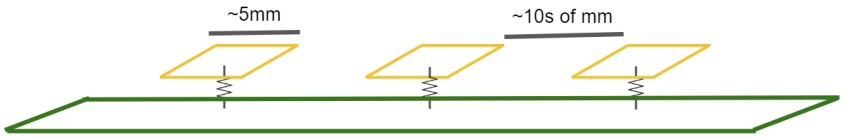

Figure 10. Strawman schematic for on-skin charge detector showing conductive fabric charge plates (yellow) resistive thread interface (black) and conductive fabric ground plane (green).

Sensors have also been previously flown to measure plasma from hypervelocity impact, including on Helios, Ulysses, Galileo, Cassini, LADEE, STEREO, MAVEN, Deep Space 1, and the Voyager planetary radio astronomy experiment. In most cases, ions and electrons were immediately subject to an external electric field, and measurements were based on total charge collected in a single channel.[41–43]

Other space-based sensing methods rely on measurements of the electromagnetic field. For instance, electric field instruments can detect dust impacts on the spacecraft body as transient pulses in spacecraft potential. This was demonstrated on the MMS 4 spacecraft in February, 2016, as the collision of a 1mm object was also detected by accelerometers, star cameras, and electric field instruments.[44] Other plasma sensing modalities include magnetic field search coils and charge detection plates.

5.2 Plasma Sensor Integration into Aerospace-Grade Textile

Plasma can be characterized on a skin by measuring charge deposition using distributed charge plates and RF emission using distributed antennas.

5.2.1 Charge deposition

In order to detect charge, we propose a dense array of conductive elements constructed either of conductive stretchable ink or embroidered conductive thread. The elements can be grounded via a resistor, and intermittent fluctuations in voltage across a resistor can be attributed to deposited charge. Separation between detection elements of tens of millimeters or smaller is recommended. We also note that charge can be measured using the space-exposed ground planes of the piezoelectric sensor - generally, charge measured by the piezoelectric sensor is sourced from within the material, whereas in this case charge would be sourced from the plasma.

The most significant impediment to this design scheme is the result shown in Figure 6 of [36] in which - at least for large mass, low velocity impactors - a plasma ejection angle of at least 30 degrees from horizontal is required for substantial charge detection. If this result holds for the low mass, high velocity regime, then only a weak charge signal on the scale of a fraction of a microcoulomb can be expected. However, a slight increase of charge from approx. 0 μC to 0.1 μC is observed when velocity is increased from 3 km/s to 5 km/s. Since based on Equation 5 charge is heavily velocity dependent, this trend presumably continues.

5.2.2 RF emission

To detect RF emission from plasma at 315 MHz, we first consider integration of an array of patch antennas into the blanket. In the domain of wearable communication, designers often opt for patch antennas due to tolerance to bending, isotropic antenna response in the exposed semisphere, and ease of textile integration. For example [45] provides a reference on designing all-textile patch antennas with microstrip feeds that can tolerate a bending radius on the order of 40mm. This antenna is manufactured using plated yarn conductive fabric as a ground plane and woolen felt as a spacer. In our case, Beta cloth itself, with dielectric constant 2.6, can be used as the antenna's substrate and conductive yarn can forms the antenna's ground plane.

Using equations and design guidelines provided in [46], a 315 MHz antenna requires a patch geometry of 30cm x 35cm x 0.2cm. Traditionally, patch antennas are not used at such low frequencies due to size constraints. To assess size constraints in this application area, we must estimate required antenna spacing.

To coarsely estimate this parameter, the expected antenna receive power must be compared to the estimated antenna sensitivity. First, to relate electric field strength to RF signal strength, we extrapolate from the previously cited measurement of 1.9 v/m field strength at a distance of 30cm from impact for a 1.4e-15 g iron particle traveling at 40km/s. Based on the relation:

$$\frac{P_T}{(4\pi d^2)} = \frac{E^2}{Z_o} \tag{6}$$

where Z_0 is the characteristic impedance of vacuum: 377 Ω, d is distance from signal emission point, E is electric field strength and P_t is transmitted power, the transmit power can be calculated as 10.8 mW for the given impact conditions. Assuming that power falls off as d^2, and, very speculatively, that each antenna can detect 1mW signals once the noise floor is considered, then antenna spacing of about 1-2 meters can be tolerated for the given particle mass and velocity. However, this calculation is not explicit about the dependence of antenna aperture on frequency.

So, more generally, we derive the following relationship between receive power and distance from impact for a narrowband antenna as a function of distance. Beginning with:

$$E = \frac{kq}{d^2} \tag{7}$$

and using charge relationship from Equation 5 we can write:

$$E = \frac{kmv^{3.8}}{d^2} \tag{8}$$

The Friis transmission formula is then used to relate power to frequency and distance from source:

$$P_R = \frac{P_T G_T G_R c^2}{(4\pi df)^2} \tag{9}$$

Finally, power is related to electric field strength via Equation 6. Using the above relations, we write receive power as a function of mass, velocity, distance from impact, and frequency:

$$P_R = \frac{k^2 m^2 v^{7.6} G_R c^2}{(4\pi)^3 d^8 Z_0 f^2} \tag{10}$$

This equation can be used as a general relationship between antenna receive power and distance from aperture for the plasma RF emission from an impactor.

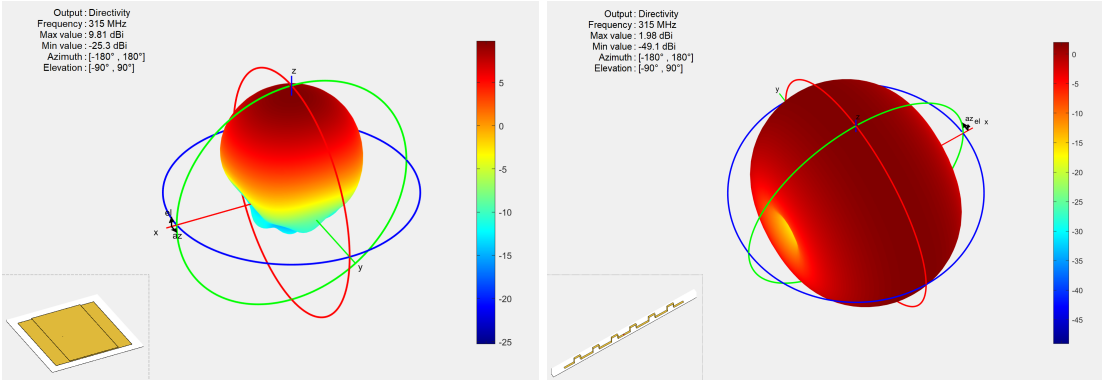

Figure 11. (Left) 315 MHz patch antenna receive pattern (Right) 315 MHz meander antenna receive pattern

Based on these approximate calculations, a 30cm x 30cm patch antenna is likely tolerable, as antenna size << antenna spacing. However, a smaller antenna design can be achieved by using a 1/4 wave trace meander antenna,

which for instance could be embroidered onto Beta Cloth using conductive yarn, though bending sensitivity would have to be taken into account. Simple models and antenna patterns were generated in MATLAB for each antenna type and showing in Figure 11. Because both the plasma origin and receive antennas will be on approximately the same plane, it is most important is to ensure reasonable antenna sensitivity at low angles relative to the x-y plane (though the plasma may continue to emit RF as it travels). The antenna receiving pattern for a patch antenna design is fairly isotropic in its space-exposed semisphere, and a gain of approximately 0 to 5 dbi can be expected at small angles. Conversely, the gain of a meander antenna is likely to range from -15dbi to -5dbi for small angles.

Finally, we note that the most significant impediment to an on-skin plasma RF sensor is the observation in prior work that surface charging to hundreds of volts is required to regularly register an emission signal, whereas surface charging is highly undesirable for spacecraft. That said, given that multiple spacecraft have detected RF emission in the past, we must conclude that surface charging relative to the ambient plasma is a frequent occurrence and/or that additional parameters are also driving RF emission.

6. CONCLUSION AND FUTURE WORK

To summarize, while electronic textiles have a rich suite of applications in the fields of medicine and human computer interaction, their uses in an aerospace context have yet to be explored. Design and engineering considerations for aerospace-grade electronic textiles were outlined. A representative application of hypervelocity impact characterization on sensate Beta cloth was then motivated. Initial prototyping demonstrated that piezoelectric yarn must be custom manufactured as a multilayer fiber, since poling of sparse PVDF filaments is infeasible. Finally, prior studies on hypervelocity plasma generation were reviewed, building to strawman designs for incorporating distributed charge and RF emission sensors on textiles. If detectable, these signatures may offer clues on the constituent ions present in the plasma, since ion composition drives electron motion.

ACKNOWLEDGMENTS

Thank you to MIT DMSE, to Dr. Hajime Yano from JAXA/ISAS, and to Sean Alden Quigg Young from Stanford.

REFERENCES

[1] Sairajan, K., Aglietti, G., and Mani, K., "A review of multifunctional structure technology for aerospace applications," *Acta astronautica* **120**, 30–42 (2016).

[2] Aglietti, G. S., Schwingshackl, C. W., and Roberts, S. C., "Multifunctional structure technologies for satellite applications," *Shock and Vibration Digest* **39**(5), 381–394 (2007).

[3] IADC, W., "Sensor systems to detect impacts on spacecraft," tech. rep., Report No. IADC-08-03 (2013).

[4] Yano, H., Hirai, T., Fujii, M., Arai, K., and Nelson, K., "Cis-lunar object detector within thermal insulation (cloth) for the 6u cubesat equuleus," in [*42nd COSPAR Scientific Assembly*], **42** (2018).

[5] Gilmore, D., "Spacecraft thermal control handbook, volume i: fundamental technologies," (2002).

[6] deGroh, K. K., Banks, B. A., and Demko, R., "Techniques for measuring low earth orbital atomic oxygen erosion of polymers," (2002).

[7] Stoppa, M. and Chiolerio, A., "Wearable electronics and smart textiles: a critical review," *sensors* **14**(7), 11957–11992 (2014).

[8] Berzowska, J., "Electronic textiles: Wearable computers, reactive fashion, and soft computation," *Textile* **3**(1), 58–75 (2005).

[9] Linton, R. C., Whitaker, A. F., and Finckenor, M. M., "Space environment durability of beta cloth in ldef thermal blankets," (1993).

[10] Dooling, D. and Finckenor, M., "Material selection guidelines to limit atomic oxygen effects on spacecraft surfaces," (1999).

[11] Graham, G., McBride, N., Kearsley, A., Drolshagen, G., Green, S., McDonnell, J., Grady, M., and Wright, I., "The chemistry of micrometeoroid and space debris remnants captured on hubble space telescope solar cells," *International journal of impact engineering* **26**(1-10), 263–274 (2001).

[12] Christiansen, E. L. and Lear, D. M., "Toughened thermal blanket for micrometeoroid and orbital debris protection," *Procedia Engineering* **103**, 73–80 (2015).
[13] Christiansen, E., Crews, J., Williamsen, J., Robinson, J., and Nolen, A., "Enhanced meteoroid and orbital debris shielding," *International Journal of Impact Engineering* **17**(1-3), 217–228 (1995).
[14] Graziosi, D. and Lee, R., "I-suit advanced spacesuit design improvements and performance testing," tech. rep., SAE Technical Paper (2003).
[15] Woodard, S. E., "Sansec sensing technologya new tool for designing space systems and components," in [*Aerospace Conference, 2011 IEEE*], 1–11, IEEE (2011).
[16] Jitsukawa, R., Hirai, T., Yano, H., Arai, K., and Nelson, K., "Computational and experimental prediction for detection of two dust populations in the earth-lunar lagrange 2 point by the equuleus-cloth system," in [*42nd COSPAR Scientific Assembly*], **42** (2018).
[17] Bauer, W., Romberg, O., Wiedemann, C., Drolshagen, G., and Vörsmann, P., "Development of in-situ space debris detector," *Advances in Space Research* **54**(9), 1858–1869 (2014).
[18] Doyle, H. M., Tom, J. G., Nogacek, K. H., Anderson, C. R., and Kang, J. S., "Design and development of dragons in-situ orbital debris detection and characterization payload," *TRANSACTIONS OF THE JAPAN SOCIETY FOR AERONAUTICAL AND SPACE SCIENCES* **59**(4), 218–225 (2016).
[19] Hirai, T., Cole, M. J., Fujii, M., Hasegawa, S., Iwai, T., Kobayashi, M., Srama, R., and Yano, H., "Microparticle impact calibration of the arrayed large-area dust detectors in interplanetary space (aladdin) onboard the solar power sail demonstrator ikaros," *Planetary and Space Science* **100**, 87–97 (2014).
[20] Sternovsky, Z., Gemer, A., Grün, E., Horanyi, M., Kempf, S., Maute, K., Postberg, F., Srama, R., and Williams, E., "Hyperdust: An advanced in-situ detection and chemical analysis of microparticles in space," in [*Aerospace Conference, 2015 IEEE*], 1–10, IEEE (2015).
[21] Dietzel, H., Eichhorn, G., Fechtig, H., Grun, E., Hoffmann, H.-J., and Kissel, J., "The heos 2 and helios micrometeoroid experiments," *Journal of Physics E: Scientific Instruments* **6**(3), 209 (1973).
[22] Bauer, W., Romberg, O., Pissarskoi, A., Wiedemann, C., and Vörsmann, P., "In orbit debris-detection based on solar panels," *CEAS Space Journal* **5**(1-2), 49–56 (2013).
[23] Nilsson, E., Lund, A., Jonasson, C., Johansson, C., and Hagström, B., "Poling and characterization of piezoelectric polymer fibers for use in textile sensors," *Sensors and Actuators A: Physical* **201**, 477–486 (2013).
[24] Hadimani, R. L., Bayramol, D. V., Sion, N., Shah, T., Qian, L., Shi, S., and Siores, E., "Continuous production of piezoelectric pvdf fibre for e-textile applications," *Smart Materials and Structures* **22**(7), 075017 (2013).
[25] Krajewski, A. S., Magniez, K., Helmer, R. J., and Schrank, V., "Piezoelectric force response of novel 2d textile based pvdf sensors," *Sensors Journal, IEEE* **13**(12), 4743–4748 (2013).
[26] Egusa, S., Wang, Z., Chocat, N., Ruff, Z., Stolyarov, A., Shemuly, D., Sorin, F., Rakich, P., Joannopoulos, J., and Fink, Y., "Multimaterial piezoelectric fibres," *Nature materials* **9**(8), 643 (2010).
[27] Mohammadi, B., Yousefi, A. A., and Bellah, S. M., "Effect of tensile strain rate and elongation on crystalline structure and piezoelectric properties of pvdf thin films," *Polymer testing* **26**(1), 42–50 (2007).
[28] Sencadas, V., Moreira, M. V., Lanceros-Méndez, S., Pouzada, A. S., and Gregório Filho, R., "α-to β transformation on pvdf films obtained by uniaxial stretch," in [*Materials science forum*], **514**, 872–876, Trans Tech Publ (2006).
[29] Cai, X., Lei, T., Sun, D., and Lin, L., "A critical analysis of the α, β and γ phases in poly (vinylidene fluoride) using ftir," *RSC Advances* **7**(25), 15382–15389 (2017).
[30] Devonshire, A., "Theory of ferroelectrics," *Advances in physics* **3**(10), 85–130 (1954).
[31] Broadhurst, M. G. and Davis, G. T., "Ferroelectric polarization in polymers," *Ferroelectrics* **32**(1), 177–180 (1981).
[32] Berger, L. I., "Dielectric Strength of Insulating Materials." Online.
[33] Permatex, "Technical Data Sheet: Permatex Dielectric Grease." AAM Revised 03/08.
[34] Lee, N., Close, S., Lauben, D., Linscott, I., Goel, A., Johnson, T., Yee, J., Fletcher, A., Srama, R., Bugiel, S., et al., "Measurements of freely-expanding plasma from hypervelocity impacts," *International Journal of Impact Engineering* **44**, 40–49 (2012).

[35] Lee, N., Close, S., Lauben, D., Linscott, I., Goel, A., Johnson, T., Yee, J., Fletcher, A., Srama, R., Bugiel, S., et al., "Measurements of freely-expanding plasma from hypervelocity impacts," *International Journal of Impact Engineering* **44**, 40–49 (2012).

[36] Crawford, D. A. and Schultz, P. H., "Electromagnetic properties of impact-generated plasma, vapor and debris," *International Journal of Impact Engineering* **23**(1), 169–180 (1999).

[37] Close, S., Colestock, P., Cox, L., Kelley, M., and Lee, N., "Electromagnetic pulses generated by meteoroid impacts on spacecraft," *Journal of Geophysical Research: Space Physics* **115**(A12) (2010).

[38] Rudolph, M., Schimmerohn, M., Osterholz, J., and Schäfer, F., "Electrical signatures of hypervelocity impact plasma with applications in in-situ particle detection," *Acta Astronautica* **101**, 157–164 (2014).

[39] Baumjohann, W. and Treumann, R. A., [*Basic space plasma physics*], World Scientific Publishing Company (2012).

[40] Bianchi, R., Capaccioni, F., Cerroni, P., Coradini, M., Flamini, E., Hurren, P., Martelli, G., and Smith, P., "Radio frequency emissions observed during macroscopic hypervelocity impact experiments," *Nature* **308**(5962), 830 (1984).

[41] Close, S., Linscott, I., Lee, N., Johnson, T., Strauss, D., Goel, A., Fletcher, A., Lauben, D., Srama, R., Mocker, A., et al., "Detection of electromagnetic pulses produced by hypervelocity micro particle impact plasmas," *Physics of Plasmas* **20**(9), 092102 (2013).

[42] Goel, A., Tarantino, P., Lauben, D., and Close, S., "Design and testing of miniaturized plasma sensor for measuring hypervelocity impact plasmas," *Review of Scientific Instruments* **86**(4), 043304 (2015).

[43] Kasahara, Y., Kasaba, Y., Kojima, H., Yagitani, S., Ishisaka, K., Kumamoto, A., Tsuchiya, F., Ozaki, M., Matsuda, S., Imachi, T., et al., "The plasma wave experiment (pwe) on board the arase (erg) satellite," *Earth, Planets and Space* **70**(1), 86 (2018).

[44] Williams, T. W., Shulman, S., Sedlak, J., Ottenstein, N., and Lounsbury, B., "Magnetospheric multiscale mission attitude dynamics: Observations from flight data," in [*AIAA/AAS Astrodynamics Specialist Conference*], 5675 (2016).

[45] Locher, I., Klemm, M., Kirstein, T., and Trster, G., "Design and characterization of purely textile patch antennas," *IEEE Transactions on advanced packaging* **29**(4), 777–788 (2006).

[46] Balanis, C. A., "Antenna theory: A review," *Proceedings of the IEEE* **80**(1), 7–23 (1992).